

CHEMISTRY

A European Journal

A Journal of



Accepted Article

Title: Liquid crystalline elastomers with gold nanoparticle cross-linkers

Authors: Michał Wójcik, Jaroslaw Wrobel, Zuzanna Janczuk, Jozef Mieczkowski, Ewa Gorecka, Joonmyung Choi, Maenghyo Cho, and Damian Pocięcha

This manuscript has been accepted after peer review and appears as an Accepted Article online prior to editing, proofing, and formal publication of the final Version of Record (VoR). This work is currently citable by using the Digital Object Identifier (DOI) given below. The VoR will be published online in Early View as soon as possible and may be different to this Accepted Article as a result of editing. Readers should obtain the VoR from the journal website shown below when it is published to ensure accuracy of information. The authors are responsible for the content of this Accepted Article.

To be cited as: *Chem. Eur. J.* 10.1002/chem.201700723

Link to VoR: <http://dx.doi.org/10.1002/chem.201700723>

Supported by
ACES

WILEY-VCH

FULL PAPER

Liquid crystalline elastomers with gold nanoparticle cross-linkers

Michał M. Wójcik*,^[a] Jarosław Wróbel,^[a] Zuzanna Z. Jańczuk,^[a] Józef Mieczkowski,^[a] Ewa Górecka,^[a] Joonmyung Choi,^[b] Maenghyo Cho,^[b] Damian Pocięcha*^[a]

Abstract: Embedding nanoparticles in a responsive polymer matrix is a formidable way to fabricate hybrid materials with pre-designed properties and prospective applications in actuators, mechanically tunable optical elements or electroclinic films. However, achieving chemical compatibility between nanoparticles and organic matter is not trivial and often results in disordered structures. Herein we show that using nanoparticles as exclusive cross-linkers in the preparation of liquid-crystalline polymers can yield long-range ordered liquid-crystalline elastomers with high loading of well dispersed nanoparticles, as confirmed with small angle XRD measurements. We also prove that our strategy to incorporate NPs as cross-linking units does not result in disruption of mechanical properties of the polymer and by the means of all-atom molecular dynamics simulations explain this phenomena. Finally, we have shown that such materials can exhibit switchable behaviour under thermal stimuli with stability spanning over multiple heating/cooling cycles. The presented strategy has proven a promising approach for the preparation of new type of hybrid liquid crystalline elastomers that can be of value for future photonic applications.

Introduction

Liquid crystal elastomers (LCEs) combine anisotropic properties of liquid crystals with the elastic properties of rubbers, they exhibit changes in their macroscopic shape due to changes in orientational order of the mesogenic units. It was shown that LCEs are able to deform reversibly in response to a variety of external stimuli, such as heat or change in chemical conditions; light was found to be especially attractive stimulus to drive changes in LCEs.¹ In the literature one can find variety of potential applications of LCEs: artificial muscles and actuators,² mechanically tunable optical elements,³ electroclinic films,⁴ smart surfaces⁵ are just few examples. Recently, new hybrid materials obtained by incorporation of inorganic nanoparticles to polymers were synthesized and studied.⁶ Embedding nanoparticles adds extra functionality to LCEs and ultimately broadens their applications as actuators, sensors and photonic devices. Nanoparticle doped LCEs can have faster response and better control over the actuation; overcoming a problem of low thermal conductivity of LCEs opens a contactless stimulation pathway to induce the anisotropic-isotropic transition by local heating.⁷ A number of different LCE materials were modified with metallic or magnetic nanoparticles. Liu et al. developed a method for dispersing gold nanospheres and gold nanorods into polyacrylate

based LCE, the obtained composites were used for building of micropillars or microactuators.⁸ Authors shown enhanced photothermal actuation behaviour of hybrid LCEs with gold nanorods inclusion less than 1 wt%. Fudouzi and Xia have demonstrated that colloidal crystals embedded in PDMS elastomer could serve as material for photonic paper and ink for color writing with colorless material.⁹ Kaiser et al. succeeded in incorporating magnetite nanoparticles into an LCE film,¹⁰ in an oscillating magnetic field the NPs vibrate, dissipation of thermal energy caused heat induced isotropisation of hybrid LCE. In this system, Fe₃O₄ particles grafted with N-oleoylsarcosine suspended in toluene were used as the solvent for LCE synthesis, no covalent bonding between particles and polymer network were created. Similar method has been presented by Schmidt and Finkelmann.¹¹ In most cases the hybrid materials are obtained by incorporating NPs into the oligomer mixture before polymerization step or by swelling of LCE with nanoparticles solution. The other approach for the functionalization of LCEs with nanoparticles has been presented by Donnio and coworkers.¹² They have synthesized a novel-type polymeric network, in which small amount of modified iron oxide nanoparticles were used as additional cross-linkers apart from conventional organic cross-linkers, however the influence of NPs on the elastomer properties was not studied in details. Both approaches are not much practical for building ordered arrays of NPs within polymer network and suffer from low nanoparticles load. The high load and ordered structure of NPs would be interesting as they may exhibit both: Lorentz-type electric permittivity and resonances in magnetic permeability, which could lead to negative refractive indexes in visible-light range. One should mention here a previous studies by Fudouzi, Kaiser and Finkelmann where the similar concept of using the nanoparticles in a composite elastomer has been explored. The difference between these concepts^{9,10,11} and the present work is we use relatively small, monodisperse and covalently attached nanoparticles. On the one hand the system studied here may be compared with all-organic polymers investigated by Wernter and Finkelmann¹³ or by Tajbakhsh and Terentjev,¹⁴ where the addition of large mass macromolecules as cross linkers had a great effect on the average effective anisotropy of polymer chains and, as a result, on the magnitude of spontaneous strain. However, the volume of cross-linkers used in these studies was much larger than the volume of gold nanoparticles used in our studies. As we have shown in our previous papers, NPs functionalized with mesogenic (or promesogenic) ligands may form complex anisotropic lattices with 2D- and 3D long-range order.¹⁵ By adjusting chemical composition of a grafting layer, metallic-dielectric stacks¹⁶ or metal columns¹⁷ can be obtained. Moreover, our recent studies show that dynamic self-assembly of silver nanoparticles, resulting from temperature-dependent changes of organic coating shape, lead to epsilon-near-zero behavior of the metamaterial.¹⁸ The future photonic applications of these systems require mechanical stability and retention of liquid crystalline behavior, so the introduction of this type of nanoparticles to polymers exhibiting liquid crystal state is crucial to achieving this goal. Here we describe a new approach toward hybrid LCEs, in which metallic nanoparticles are used as exclusive cross-linking agents for polymer backbones. The strategy allows to introduce large number of gold nanoparticles into polymer matrix and assures that

[a] Michał M. Wójcik, Jarosław Wróbel, Zuzanna Z. Jańczuk, Józef Mieczkowski, Ewa Górecka, Damian Pocięcha
Faculty of Chemistry
University of Warsaw
1 Pasteur str, 02-093 Warsaw, Poland
E-mail: pociu@chem.uw.edu.pl, mwojcik@chem.uw.edu.pl

[b] Joonmyung Choi, Maenghyo Cho
School of Mechanical and Aerospace Engineering
Seoul National University
1 Gwanak-ro, 1 Gwanak-gu, 08826 Seoul, Korea

Supporting information for this article is given via a link at the end of the document.

FULL PAPER

each particle is covalently attached to the polymer backbone, therefore prevent their uncontrolled aggregation. Moreover, use of the nanoparticles functionalized with mesogenic ligands significantly improves the whole system compatibility.

Results and Discussion

Materials properties. The gold nanoparticles were prepared using modified Brust method,¹⁹ the procedure yield particles with mean diameter 2.2 nm (+/- 0.4 nm), covered with n-octyl thiols attached covalently to a metal surface (**GNP@C8**).

In the next step NPs grafting layer was modified by ligand-exchange reaction, in which ca. 30% of n-alkyl thiols were replaced by mesogenic olefin ligands **L2** (for the details see Experimental section). The molecular structure of **L2** (Figure 1) with three ring mesogenic core, is similar to (pro)mesogenic ligands used in our previous studies that drove the NPs into the long range ordered assemblies.^{15,19} The ligand **L2** has the double bond at the end of terminal chain to ensure covalent bonding to siloxane backbone. The TEM images of the **GNP@L2** sample revealed a relatively narrow size distribution of NPs with the average diameter of the gold core 2.2 nm (+/-0.4 nm; for corresponding size distribution histogram see SI Figure S6). The toluene suspension of **GNP@L2** could be stored at room temperature even for several weeks without clouding and/or precipitation. The modified nanoparticles showed good miscibility with LC matrices even at high concentration, in

contrast to native particles **GNP@C8** that easily agglomerated at similar conditions. Good compatibility of **GNP@L2** with LC matrix was proven by studying behavior of supernatant from the purifications process (**MIX1**) - a mixture of small gold nanoparticles, mesogenic compound **L2** and bromine derivative **L2-Br**. After evaporation of solvent and temperature annealing the SAXS measurements proved that NPs are well dispersed as there were no diffraction signals coming from the aggregated nanoparticles.

In AFM measurements the **MIX1** sample exhibited interesting morphology with arrays of stripes (Figure 2) of ~50 nm periodicity, an order of magnitude larger than molecular length.

SEM-EDS measurements showed that nanoparticles are not located in any particular place of the sample, but homogeneously distributed within the composite (Figure S7). The TEM imaging revealed that nanoparticles **GNP@L2** have clear tendency toward formation of a lamellar structure, the average distance between the layers is 8-9 nm (Figure 3a). The lamellar structure was confirmed also by X-ray diffraction experiments; for sample aligned by shearing the pattern typical for lamellar phase was obtained at T = 30 °C (Figure 3b), with a series of commensurate sharp reflections related to the layer thickness, 8.2 nm, positioned along common azimuthal direction (layer normal) and a diffused signal on equatorial, reflecting the mean interparticle distance, ~3 nm, inside the layers. The measured layer periodicity was comparable to the value determined from TEM images. Upon annealing additional electron density modulation along the layers developed, evidenced by

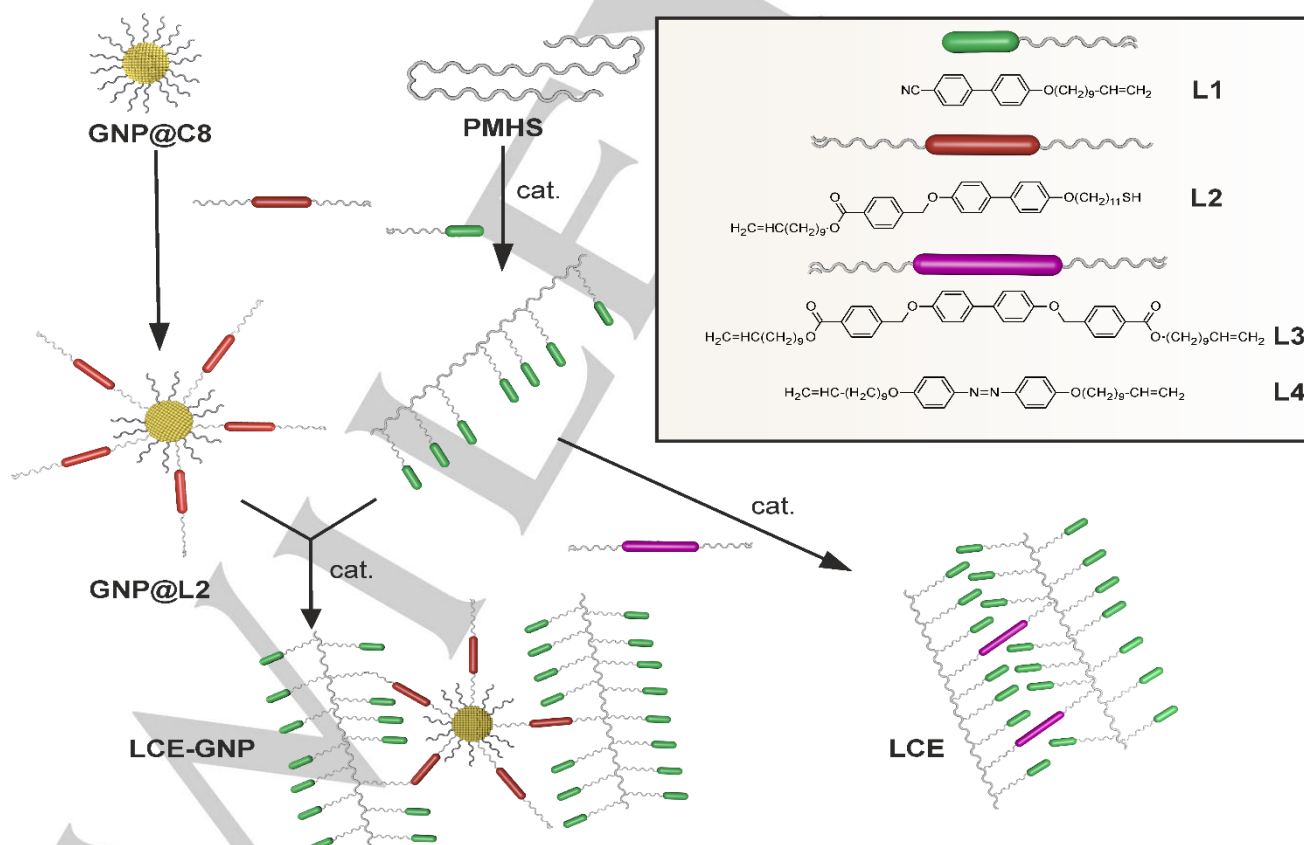


Figure 1. General scheme of preparation of a gold nanoparticle cross-linked elastomers (**LCE-GNP**). PMHS based prepolymer with mesogenic units **L1** was cross-linked by gold nanoparticles functionalized with double bond terminated mesogenic ligands (**GNP@L2**). For comparison also all-organic elastomers were obtained from the same prepolymer and double-olefin terminated rod-like cross-linkers (**L3** or **L4**).

FULL PAPER

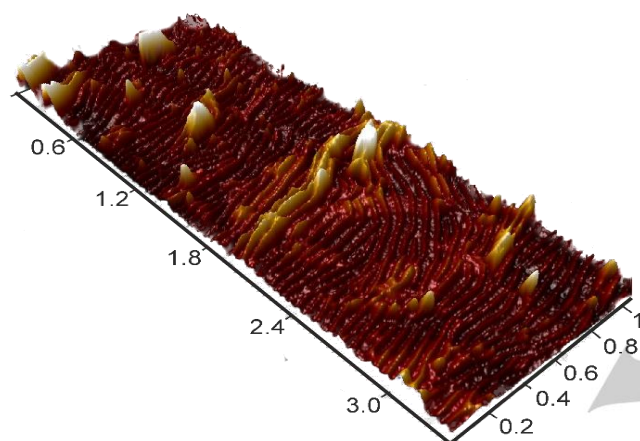
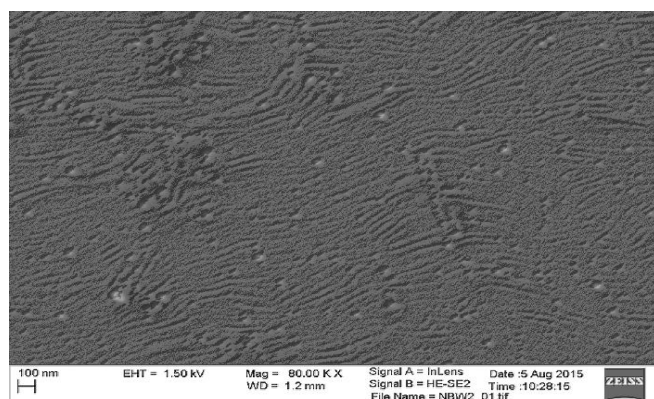


Figure 2. SEM and AFM images of nanoparticles and ligands composite (**MIX1**) constituent of 15% of **GNP@L2**, 5% of **L2** and 80% of **L2Br** ligand.

appearance of new diffraction signals on the XRD pattern (Figure S8). The lamellar phase melted to isotropic liquid around 115 °C. Upon further heating (>160°C) the nanoparticles start to decompose.

Simultaneously, we conducted synthesis of simple olefin cyanobiphenyl derivative **L1**, to be used as a pendant unit in the elastomer, and organic cross-linkers with olefin groups at both molecular ends, having three- or two-ring mesogenic cores, **L3** and **L4**, respectively (Figure 1), for preparation of reference, all-organic, elastomer materials. Cyanobiphenyl derivative **L1**, ligand **L2** and cross-linkers **L3** and **L4** were investigated for mesogenic behaviour; except for azo derivative **L4** they all formed LC phases (Table. 1).

The compound **L1** exhibited partially bilayer smectic A_d phase ($d \sim 36$ Å, $d/L \sim 1.5$) with clearing temperature 75°C, compound **L2** formed two tilted smectic phases, SmI and SmC, and showed clearing temperature 148°C, for compound **L3** a sequence of three tilted smectics, SmJ - SmI - SmC was observed with clearing point 195°C.

As a polymer backbone the commercially available poly(methylhydrosiloxane) (PMHS) was used having average $M_n = 1700-3200$ g mol⁻¹. Two hybrid liquid crystalline elastomers were synthesized with **L1** pendant and gold particles **GNP@L2** as cross linker (Figure 1, Table 1), differing in concentration of gold nanoparticles – **LCE-GNP1** (with ~ 0.5% of **GNP@L2**) and **LCE-GNP2** (with ~2% of **GNP@L2**). For comparative studies also two all-organic elastomers were obtained, **LCE-L3** and **LCE-L4**, cross-linked via **L3** and **L4**, respectively (Figure 1, Table 1).

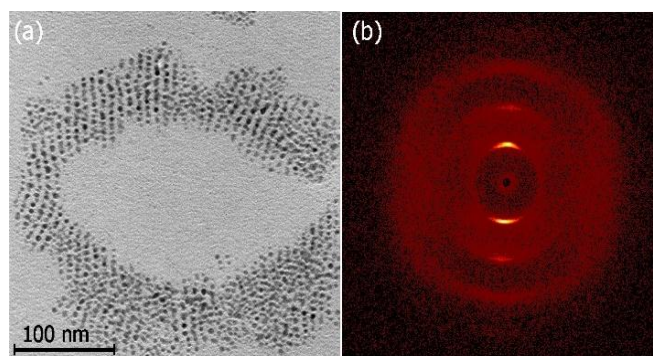


Figure 3. (a) TEM image of **GNP-L2** nanoparticles showing their tendency toward formation of lamellar structures, (b) SAXRD pattern obtained at T=30 °C for aligned sample of **GNP-L2**.

In the control experiment a polymer with **GNP@L2** cross-linker but without mesogenic ligand **L1**, was also prepared, in this case amorphous material with no liquid crystalline order was formed (Figure S9), providing an evidence that **GNP@L2** can cross-link polysiloxane backbones. The thermogravimetric studies were conducted in order to evaluate thermal stability of prepared polymers. All polymers showed onset of decomposition ~400°C, except for the **LCE-L4** containing azo-based cross-linker, which exhibited lower onset of decomposition ~250°C (Figures S10, S11 and S12). The presence of nanoparticles does not affect the thermal stability of the polymers. Moreover, TGA analysis showed that the siloxane part, remaining after heating the sample to ~600°C, was about 20% by weight for all composite materials. The composition of polymer samples was also studied by XPS method (see SI, Figures S13, S14 and S15). For all elastomers Si2p, Si2s, C1s and O1s peaks were observed, for hybrid elastomers **LCE-GNP1** and **LCE-GNP2** presence of gold was

	Composition	Phase sequence
L1		Cr 57.8 (97.9) SmA 74.23 N 75.6 (6.6) Iso
L2		Cr 70.9 (41.3) SmI 136.9 (9.2) SmC 145.4 (22.1) Iso
L3		Cr 79.0 (56.3) SmJ 137.1 (5.6) SmII 167.3 (2.1) SmC 193.0 (24.1) Iso
L4		Cr 91.7 (62.8) Iso
LCE1	95% of L1 and 5% of L3	Cr 39.0 (5.4) Sm 159.8 (2.3) Iso
LCE2	95% of L1 and 5% of L4	Cr 39.9 (19.3) Sm 152.8 (5.1) Iso
LCE-GNP1	99.5% of L1 and 0.5% of GNP@L2	Cr 46.6 (23.5) Sm 158.2 (4.8) Iso
LCE-GNP2	98% of L1 and 2% of GNP@L2	Cr 41.5 (40.9) Sm 152.5 (6.0) Iso
LCE-GNP-Mix	LC composite: 15% of GNP@L2 + 5% of L2 + 80% of L2Br	

Table 1. Physicochemical and structural characteristics of mesogenic ligands, LCE's and LCE-GNP. Transition temperatures (in °C) and thermal effects (in brackets, Jg⁻¹) were determined from DSC thermograms (second heating scan).

FULL PAPER

additionally detected by appearance of Au4f signal (Figure S15). The gold chemistry in hybrid elastomers determined from XPS scans was very similar to that observed previously for a nanoparticle system²⁰ (inset in Figure S15), as expected there were no changes in the bonding between L2 ligand and metallic surface induced by the polymerization procedure. The successful incorporation of the gold nanoparticles into elastomer network, was indirectly evidenced by scanning electron microscopy (SEM) imaging. Due to the presence of relatively large content of well dispersed conducting metallic nanoparticles, SEM pictures of **LCE-GNP** samples could be easily recorded (Figure 4) without metal sputtering or other sample pretreatment, in contrast with SEM studies of the common all-organic polymers.

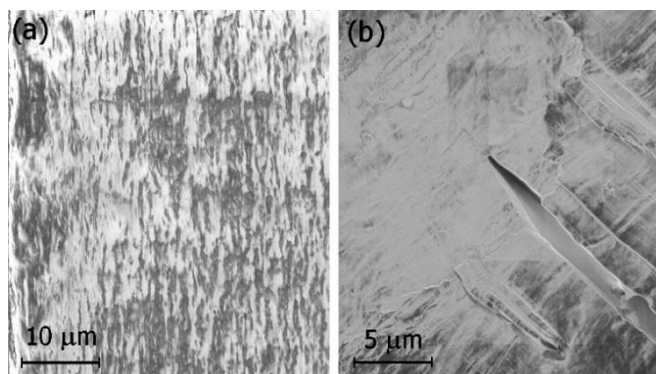


Figure 4. SEM images of hybrid polymer **LCE-GNP1** for two different places.

The hybrid polymers **LCE-GNP1** and **LCE-GNP2** showed grainy non-characteristic weakly birefringent optical textures (Figure S16), the DSC and XRD studies clearly revealed presence of smectic phase in broad temperature range for both materials. The DSC thermograms showed two temperature events: melting at 50°C and clearing at 150°C (Figure 5) for all polymeric materials.

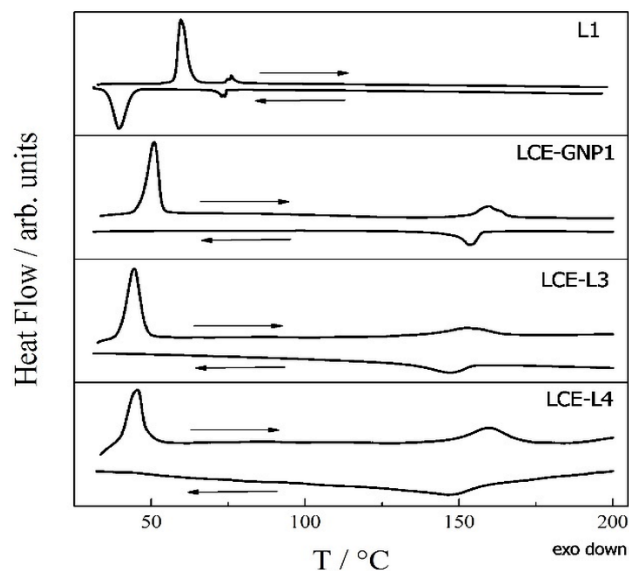


Figure 5. DSC thermograms recorded on first heat/cool cycle for monomer **L1** and polymers with different types of cross-linkers.

The X-ray patterns evidenced lamellar structures for both polymers: **LCE-GNP1** and **LCE-GNP2**, the layer spacing, d , changed in a range 39 – 44 Å with negative thermal expansion coefficient -0.04 ÅK^{-1} for both polymers (Figure 6). The observed smectic layer thickness of **LCE-GNP** was significantly larger than for monomeric compound **L1**, apparently in the polymers a bilayer structure with d corresponding to double molecular length of pendant units is formed. For both elastomers the diffused XRD signal was observed at high angle range, corresponding to 4.5 Å, reflecting the liquid like order of mesogens within the smectic layers. The X-ray patterns do not change significantly in consecutive heating/cooling scans, showing that the NPs remain well dispersed in the polymer network. For **LCE-GNP2** at room temperature onset of crystallization was also observed, marked as an appearance of a few sharp reflections at high diffraction angle range (SI Figure S17). Very homogeneous distribution of nanoparticles in polymer network was evidenced for both hybrid elastomers by strong X-ray scattering at low angles and lack of the diffraction signal observed in our previous studies^{15,16a,21} related to mean interparticle distance (Figure 6). Strong, slowly decaying isotropic scattering around direct beam visible in a pattern for smectic phase **LCE-GNP** indicates presence of non-aggregated gold nanoparticles, well dispersed in polymer matrix. Neither intensity nor angular distribution of small angle scattering changed at LC-Iso phase transition, nor was affected by consecutive heating/cooling runs. This shows that chemical bonding of NPs in polymer network effectively prevents their agglomeration.

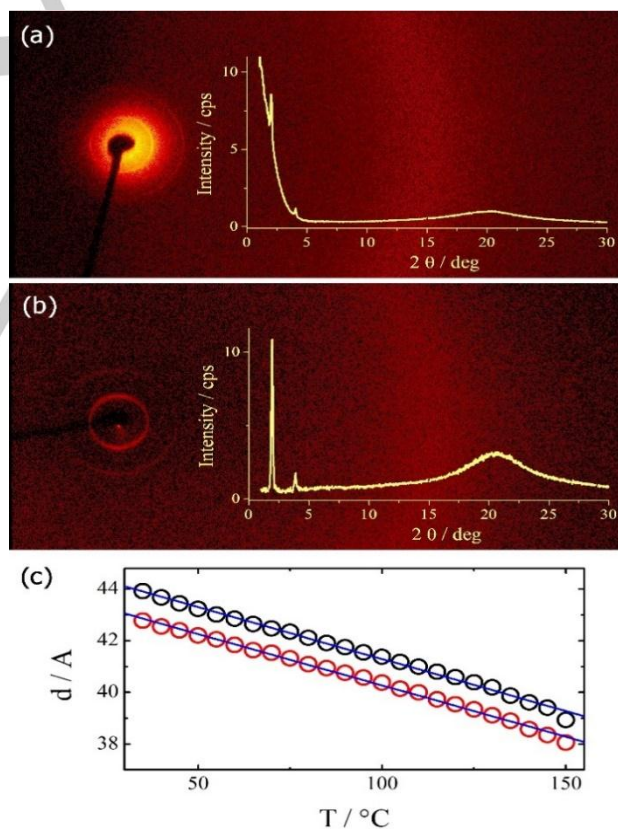


Figure 6. 2D XRD patterns taken in broad angle range for smectic phases of polymers: (a) **LCE-GNP2** with hybrid cross-linker and (b) **LCE-L3** with all-organic cross-linker. (c) temperature dependence of smectic layer thickness for **LCE-GNP2** (black circles) and **LCE-L3** (red circles), both were fitted to linear dependence yielding similar thermal expansion coefficient, -0.04 ÅK^{-1} .

FULL PAPER

All-organic elastomers **LCE-L3** and **LCE-L4** prepared from the same polymer back-bone and mesogenic pendants **L1**, exhibited phase behavior similar to the hybrid polymers, **LCE-GNP**. They formed smectic phase stable up to $\sim 159^\circ\text{C}$ for **LCE-L3** and 152°C for **LCE-L4** (Figure 5, Figure 6b and SI Figure S18). The layer spacing for **LCE-L3** was close to that observed for hybrid elastomers, it also changed with temperature with the same expansion coefficient (Figure 6c). It was noticed that the **LCE-GNP** elastomers could be easily swollen with excess of **L1** molecules. Upon admixture of up to several wt% of the ligand molecules, the layer spacing grows to $\sim 50\text{-}54$ Å; the lack of the separate X-ray signal related to smectic phase of **L1** compound shows that unbound ligand molecules are well dispersed in the polymer network and do not separate from the matrix. Interestingly, presence of free ligand molecules enhances the tendency of elastomer to crystallize at room temperature, partial re-crystallization was observed for swollen **LCE-GNP1**, while non-swollen polymer showed LC state at ambient conditions even for weeks. Finally, it is worth to mention that elastomers with NP cross linkers do not have typical rubber elasticity at room temperature, they form rather soft 'plastics'. The rubber elasticity is recovered upon heating above 50°C .

Computational results

The equilibrated all-atom simulation models for the all-organic (neat) and hybrid LC elastomers are shown in Figure 7. At room temperature, it was found that the orientational order of the cyanobiphenyl mesogens is preserved after the incorporation of gold nanoparticles into polymer network. Therefore, the **LCE-GNP** nanostructure still exhibits an anisotropy in elastic moduli, as shown in Figure 8. The obtained stress-strain relations were nearly identical for the hybrid elastomer and the reference, all-organic one, although the local conformation of elastomer chains around the NP is significantly disturbed due to the high adsorption energy of the gold atoms at the NP surface. In the simulation it was also found that the insertion of gold nanoparticles drastically changed both, the density and free volume distributions of the polymer chains, in result the associated self-diffusion characteristics were affected (the quantitative calculation results are given in SI in Figures S19, S20, and S21). The disturbance of local order of polymer chains near the NP surface is compensated by the reinforcing effect of gold NPs and their associate thiol-gold bonds, thus the mechanical response of the material remained unchanged.

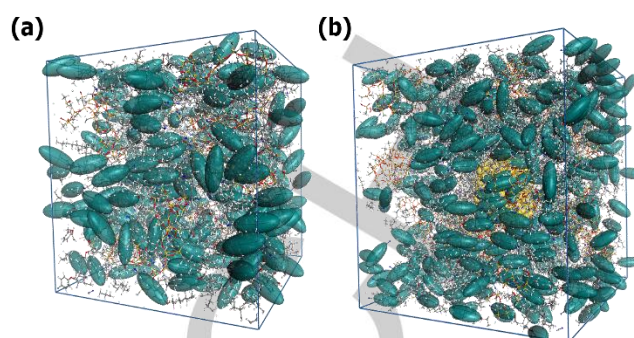


Figure 7. Equilibrated periodic unit cell of (a) the all-organic (neat) LCE and (b) the LCE-GNP. The cyanobiphenyl units are highlighted in green.

Computational verification section (Molecular Dynamics Simulation Setup). The 3D atomic structure of LCE and LCE nanocomposites reinforced with gold clusters were modeled by commercial MD software, Materials Studio 6.0 (Accelrys Inc.) with the polymer-consistent force field (PCFF).²² The non-bond cutoff distance was set to 9.5 Å. Regarding the LCE-GNP nanocomposites model, thiol-gold interaction was additionally considered by adding stretching, bending, and dihedral force field parameters for the involved atoms. The force field parameters were extracted from the study by Guberman-Pfeffer et al.²³ and are listed in the SI (See Table ST 1).

Unit Cell Model Preparation. Neat LCE unit cell and LCE nanocomposites reinforced with GNP (LCE-GNP) unit cell models were prepared for MD simulations. The modeling procedure of liquid crystalline elastomers followed our previous works.²⁴ Poly(methylhydrosiloxane) backbone (molecular weight: 2407.10 g/mol), 2.2 nm GNP, cross-linker, mesogenic ligands and cyanobiphenyl derivative were independently modeled and collocated into a periodically bounded amorphous unit cell. The orientation of the cyanobiphenyl derivatives were initially preserved along the x-axis in order to describe the uniaxial LC phase. The interatomic potential energies of the unit cells were minimized using the conjugated gradient method (convergence cutoff of 0.1 kcal/mol·Å), followed by the NVT (isothermal) ensemble simulation at 300K for 2 ns, and the NPT (isothermal and isobaric) ensemble at 300K and 0.1 MPa for 3 ns. Using the Verlet algorithm, the equations of

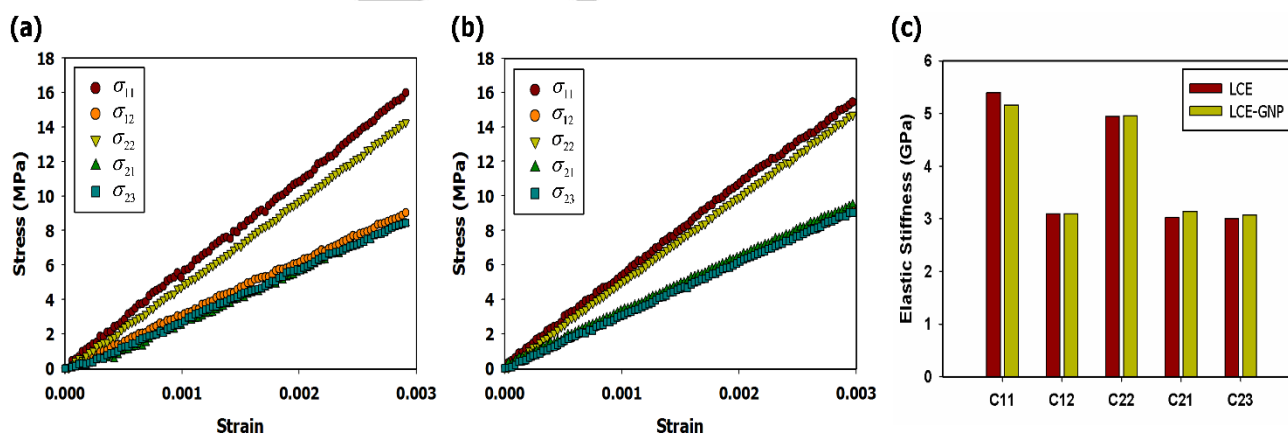


Figure 8. Elastic stress-strain relations obtained in MD simulations for (a) neat LCE and (b) hybrid LCE-GNP. (c) comparison of elastic stiffness of modelled elastomers.

FULL PAPER

motion were integrated with a time step of 1.0 fs. Details of the composition of LCE and LCE-GNP are listed in the SI (see **Figure S4** and **Table ST 2**).

Crosslinking Simulation. After the two models were equilibrated in the NPT ensemble, the cyanobiphenyl derivatives and ligand molecules were covalently bonded to the backbone chain of PMHS. To simulate the crosslinking reaction in classical MD, we artificially create new covalent bonds when the interatomic distances between the reactive sites of the molecules are within the designated cutoff condition.²⁵ The cutoff starts at the value of 4Å, and gradually increases with the step increment of 0.5Å until the maximum value does not exceed 6.0Å. During the crosslinking simulation, the potential energy components are newly updated and the atomic structure is repeatedly relaxed using a conjugated gradient method, followed by NVT ensemble simulation at 300K for 300 ps. The final crosslink density of cured cyanobiphenyl derivatives is 0.41. The local conformation of elastomeric networks and the associated distribution of mesogenic molecules for neat LCE and LCE-GNP nanocomposites are presented in **Figure 9**.

Uniaxial Tensile Loading Simulations. The mechanical stresses of the considered microstructures can be computed with the virial stress tensor (σ) defined as,

$$\sigma = \frac{1}{V} \left(-\sum_i^N m_i (\mathbf{v}_i \mathbf{v}_i) + \frac{1}{2} \sum_i^N \sum_{j \neq i}^N \mathbf{r}_{ij} \mathbf{F}_{ij} \right) \quad (1)$$

where V is the volume of the unit cell, N is the total number of atoms, m and v are the mass and the thermal velocity of i -th atom, r and F are the relative position and the atomic force between atoms i and j , respectively. To derive the continuum (Cauchy) stress, firstly the two models were relaxed under near-zero temperature (0.1K) for 500 ps within the NVT ensemble.²⁵ Since the temperature condition was close to 0 K, only the potential energy term in eq. (1) appear and the thermal energy on the kinetics of the molecules is excluded. After the relaxation process, the uniaxial tensile loading simulations were carried out along x , y , and z directions by elongating the lattice length of the unit cell under NVT ensemble with the true strain rate of $10^{-6}/\text{ps}$. Under linear deformation, the unit cell model follows Hooke's law so the elastic constants can be described as:

$$\sigma = \mathbf{C} \epsilon \quad (2)$$

where \mathbf{C} is the stiffness tensor and ϵ is the normal strain. In order to minimize computational uncertainty caused by initial velocity distribution of the atoms in MD simulations, all of the elastic constants were averaged over five different simulation results. The mechanical loading simulations were carried out using the LAMMPS code (Sandia Lab.).

Conclusions

In these preliminary studies, the objective was to demonstrate the possibility of homogeneous incorporation of the nanoparticles into polymer network as cross-linking agents. The new type liquid crystalline elastomers with gold NP based cross-linkers were obtained. This is promising approach for obtaining elastomers with high metal load and good thermal stability. The thermal stability and phase properties of hybrid elastomers are similar to reference polymers in which organic cross-linkers were used. Chemical bonding of NPs in polymer network ensured their stable dispersion and prevented their agglomeration even after multiple temperature cycling through the clearing/melting temperature. Protection against aggregation and uniform dispersion of nanoparticles in the polymer allows nanoparticle retain their individual properties, which are crucial from the point of view of their photonic applications. Due to the multivalent nature of NP cross-linkers the elastomers are at room temperature relatively stiff, in future work the rubber elasticity could be tuned by controlling the number of olefin ligands at the NPs surface. MD simulations showed that introduction of spherical inorganic nanoparticles into elastomer network does not disturb mechanical properties of the material, despite changes in the local order of polymer chains near the particle surface.

Overall, this work provides a novel pathway for the preparation of a new type of highly flexible liquid crystalline polymers with high metal load for future applications, as e.g. epsilon-near-zero metamaterials. The introduction of larger gold or silver plasmonic nanoparticles in polysiloxane is highly relevant for photovoltaics as it may enhance optical absorption.

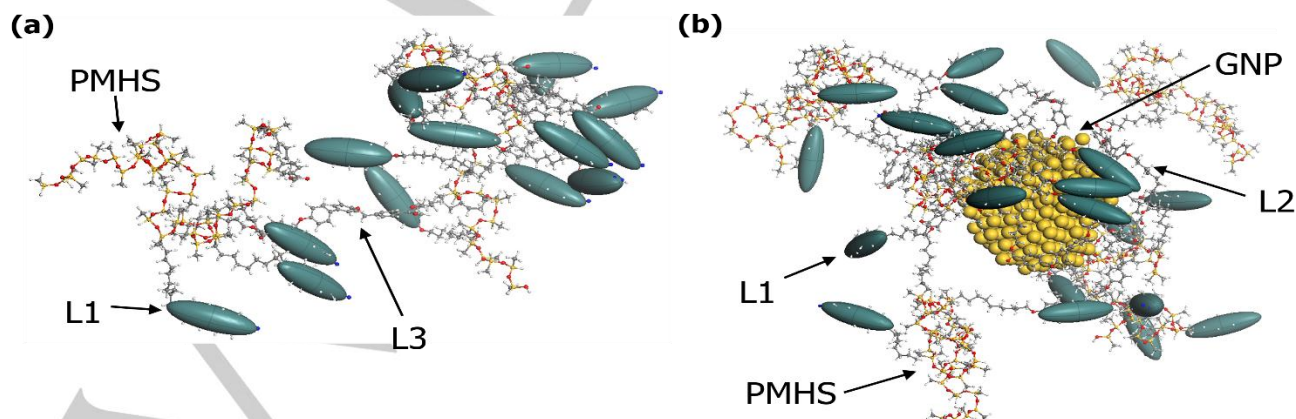


Figure 9. Crosslinking scheme of the elastomeric networks between PMHS backbone chains in all-atom simulations: (a) The neat LCE and (b) the LCE-GNP models.

FULL PAPER

Experimental Section

Organic synthesis. Synthesis of used ligands, cross-linkers and ligand for the functionalization of gold nanoparticles is described in SI. Solvents and substrates were obtained from Sigma-Aldrich. Before use, all solvents were dried over thermally activated molecular sieves. All reactions, except LCE and LCE-GNP preparation and purification, were carried out under nitrogen atmosphere in dried glassware. Purification of reaction products was carried out by column chromatography using Sigma Aldrich silica gel 60Å (230-400 mesh) at atmospheric pressure or by crystallization if possible. Yields refer to chromatographically and spectroscopically (^1H NMR) homogeneous materials. The ^1H NMR and ^{13}C NMR spectra were recorded at either 200 MHz or 500 MHz NMR Varian Unity Plus.

Proton chemical shifts are reported in ppm (δ) relative to the internal standard – tetramethylsilane (TMS $\delta=0.00$ ppm). Detailed synthetic procedures and analyses are given in the SI (Figures S1, S2, S3).

Nanoparticles synthesis. Gold NPs were synthesized according to the modified Brust procedure.¹⁹ Briefly, AuCl_3 in diluted HCl (1.7 mL of a solution - 30% Au content, from Sigma-Aldrich), was dissolved in 90 mL of distilled water and transferred into toluene with tricaprylmethylammonium chloride (5.0 g dissolved in 250 mL of toluene). The resulting organic phase was then separated, cooled down to 4°C and stirred with octane thiol (0.5 mL). Reduction was performed using an excess of sodium borohydride (1.2 g). After stirring at room temperature for 1h, the organic phase was collected, washed with distilled water and concentrated to ca. 5 mL. The resulting dark solution was suspended in 200 mL of ethanol, cooled down to 4°C and centrifuged (5 min.; 1000RPM). The black deposit was dissolved in a small amount of toluene (5 mL). The washing procedure with ethanol was repeated twice. The purification process and the refinement is based on the partial precipitation of well dispersed nanoparticles utilizing mixtures of ethanol and acetone. The dark brown precipitate obtained after synthesis of nanoparticles was sonicated for 60 s and centrifuged (5 min, 13 000 rpm) in 15 mL of toluene. In the next step, the toluene solution was precipitated with acetone-ethanol mixture (80 mL, 1:1) and centrifuged (3 min, 8 000 RPM in 35°C). Again precipitate was dissolved in a small amount of toluene (10 mL), precipitated with acetone-ethanol (100 mL, 1:2) and centrifuged. The procedure was repeated twice. The black precipitate was collected and used for ligand exchange reaction.

Ligand exchange reaction on nanoparticles. Octyl thiol coated NPs (**GNP@C8**) were used for the preparation of hybrid NPs (**GNP@L2**). To 25 mg of NPs dissolved in 15 mL of toluene 20 mg of a mesogenic ligand (**L2**) was added. The reaction proceeded at room temperature for 36 h. Then, NPs were precipitated with 20 mL of acetone-ethanol mixture (1:2) and centrifuged. The supernatant containing free thiol ligand molecules was collected and named as **MIX1**. The precipitate was dissolved in 10 mL of toluene and centrifuged (5 min, 13 000 rpm). This washing procedure was repeated until no traces of free mesogenic ligand remained, as determined by thin layer chromatography. The concentration of nanoparticles was estimated via simple weight method. Gold nanoparticles obtained in Brust method are relatively high concentrated and can be easily purified in both cases: after the synthesis or after ligand exchange in combination with complete purification from the ligand excess. Briefly, a 0.25 mL toluene solution of gold nanoparticles was placed in a carefully weighed weighing vessel. After the solvent evaporation in 110°C the vessel was weighted again on the precision scale and the concentration was calculated and estimated as 4.6 mg/mL for **GNP@C8** and 2.3 mg/mL for **GNP@L2**. Both solutions were sealed, stored in 4°C and used as prepared for future experiments.

LCE preparation. In order to obtain the LCE's we applied a protocol used by Finkelmann and other authors.²⁶ The poly(methylhydrosiloxane), cross-linker and mesogenic ligands were used. The resulting material was partially oriented by means of mechanical stress. The application of the mechanical stress is a common method, the use of which has been initiated in the aforementioned early works of Finkelmann. In the case of described substances, the orientation was introduced analogously to modified procedure described by Zentel and coworkers,²⁷ where spin casting

method was used. In the first step the PMHS was dissolved in dried toluene, then an appropriate amount of mesogenic ligand and a platinum catalyst was added. The next step was cross-linking the polysiloxane chains using the **GNP@L2**, **L3** or **L4** (Fig. 1), the process was carried out at temperature of 75-80°C, constantly maintaining the centrifugation of the reaction mixture. In the final stage, the excess of unreacted ligand was removed by repeated washings with dried toluene.

XRD measurements. The small-angle X-ray diffraction (SAXRD) studies have been carried out using Bruker Nanostar diffractometer (CuK_α radiation (wavelength 1.54 Å), parallel beam formed by cross-coupled Goebel mirrors and three pinhole collimation system, MRI TCPU-H heating stage, Vantec 2000 area detector). Samples of **GNP-L2** were prepared as thin films on a kapton tape and aligned by mechanical shearing at elevated temperature. Samples of polymers were measured in transmission, without substrates. The X-ray diffraction patterns in wide angle range were collected using a Bruker GADDS system (CuK_α radiation, parallel beam formed by Goebel mirror and two pinhole collimator, Vantec 2000 area detector, equipped with modified Linkam heating stage).

Differential scanning calorimetry (DSC). Phase transition temperatures and associated enthalpy changes for all organic compounds and elastomers were determined with differential scanning calorimeter, TA Q200. The samples of 2–5 mg were placed into aluminum pans and kept in nitrogen atmosphere during measurements. Cooling and heating rates of 10 K min^{-1} were applied.

Transmission electron microscopy. Transmission electron microscopy was performed using Zeiss Libra 120 microscope, with LaB6 cathode, equipped with OMEGA internal columnar filters and CCD camera. For TEM imaging materials were dropcasted onto TEM carbon coated copper grids and thermally annealed at 90 °C.

Scanning electron microscopy (with EDS). The samples were analyzed using of a FE-SEM Merlin (Zeiss, Germany) instrument. The chamber pressure was 1.10^{-5} Torr, and pictures were registered for 3- and 15-kV electron beam. Before exposing the samples to the electron beam, they were dried under vacuum for 24h.

Thermogravimetric analysis (TGA). Thermogravimetric analysis were performed with a TA Q50 V20.13 analyzer. The measurements were carried out in 100-600 °C range with 10 K min^{-1} heating rate in air. Prior the measurement samples were conditioned at 100°C for 20 min.

Acknowledgements

Supporting Information

Synthesis and characterization of materials, additional experimental results: SEM, XRD, TGA, XPS, optical microscopy. Structural properties obtained from MD simulations: Model composition for modeling, radial density distribution, free volume distribution, mean squared displacement.

Funding Sources

The work was supported by NCN (Poland) grants no: UMO-2013/08/M/ST5/00781 (DP) and UMO-2014/15/D/ST5/02570 (MW).

The work was supported by NRF (Korea) grants no: 2012R1A3A2048841 (MC).

Keywords: Liquid crystals • Nanoparticles • Liquid crystal elastomers • Nanostructures • Surface chemistry

[1] a) R. Eelkema, M. M. Pollard, J. Vicario, N. Katsonis, B. S. Ramon, C. W. M. Bastiaansen, D. J. Broer, B. L. Feringa, *Nature* **2006**, *440*, 163; b) E. K. Fleischmann, R. Zentel, *Angew. Chem. Int. Ed.* **2013**, *52*, 8810-8827; c) R. R. Kohlmeier, J. Chen, *Angew. Chem. Int. Ed.* **2013**, *52*, 9234-9237; d) S. Iamsaard, S. J. Alshoff, B. Matt, T. Kudernac, J. J. L. M. Cornelissen, S. P. Fletcher, N. Katsonis, *Nat. Chem.* **2014**, *6*, 229-235, e) H. Jiang, S. Kelch, A. Lendlein, *Adv. Mater.* **2006**, *18*, 1471-1475.

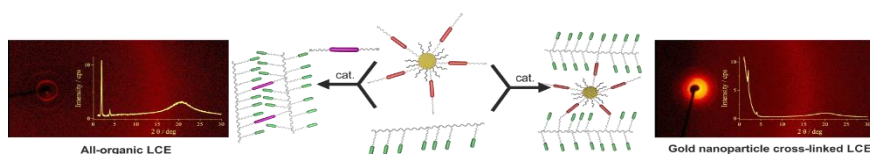
FULL PAPER

- [2] a) T. Ikeda, J. I. Mamiya, Y. L. Yu, *Angew. Chem. Int. Ed.* **2007**, *46*, 506-528; b) M. Yamada, M. Kondo, J. I. Mamiya, Y. L. Yu, M. Kinoshita, C. J. Barrett, T. Ikeda, *Angew. Chem. Int. Ed.* **2008**, *47*, 4986-4988; c) H. Yu, T. Ikeda, *Adv. Mater.* **2011**, *23*, 2149-2180.
- [3] a) J. Schmidtke, S. Kniesel, H. Finkelmann, *Macromolecules* **2005**, *38*, 1357-1363; b) S. Schuhladen, F. Preller, R. Rix, S. Petsch, R. Zentel, H. Zappe, *Adv. Mater.* **2014**, *26*, 7247-7251.
- [4] C. M. Spillmann, J. H. Konnert, J. R. Deschamps, J. Naciri, B. R. Ratna, *Chem. Mater.* **2008**, *20*, 6130-6139.
- [5] H. Yang, A. Buguin, J. M. Taulemesse, K. Kaneko, S. Mery, A. Bergeret, P. Keller, *J. Am. Chem. Soc.* **2009**, *131*, 15000-15004.
- [6] a) Ch. Li, Y. Liu, X. Huang, H. Jiang, *Adv. Funct. Mater.* **2012**, *22*, 5166-5174; b) R. Montazami, Ch. M. Spillmann, J. Naciri, B. R. Ratna, *Sensors and Actuators A*, **2012**, *178*, 175-178; c) Y. Chen, T. Gan, Ch. Ma, L. Wang, G. Zhang, *J. Phys. Chem. B*, **2016**, *120*, 4715-4722; d) Ch. Feng, X. Pang, Y. He, Y. Chen, G. Zhang, Z. Lin, *Polym. Chem.* **2015**, *6*, 5190-5197; e) M. Zhong, R. Wang, K. Kawamoto, B. D. Olsen, J. A. Johnson, *Science*, **2016**, *353*, 1264-1268.
- [7] Y. Ji, J. E. Marshall, E. M. Terentjev, *Polymers* **2012**, *4*, 316-340.
- [8] X. Liu, R. Wei, P. T. Hoang, X. Wang, T. Liu, P. Keller, *Adv. Funct. Mater.* **2015**, *25*, 3022-3032.
- [9] H. Fudouzi, Y. Xia, *Adv. Mater.* **2003**, *15*, 892-896.
- [10] A. Kaiser, M. Winkler, S. Krause, H. Finkelmann, A. M. Schmidt, *J. Mater. Chem.* **2009**, *19*, 538-543.
- [11] M. Winkler, A. Kaiser, S. Krause, H. Finkelmann, A. M. Schmidt, *Macromol. Symp.* **2010**, *291-292*, 186-192.
- [12] A. Garcia-Marquez, A. Demortiere, B. Heinrich, D. Guillon, S. Begin-Colin, B. Donnio, *J. Mater. Chem.* **2011**, *21*, 8994-8996.
- [13] H. Wermter, H. Finkelmann, *e-Polymers*, **2001**, *13*
- [14] A. R. Tajbakhsh, E. M. Terentjev, *Eur. Phys. J. E.* **2001**, *6*, 181-188.
- [15] W. Lewandowski, M. Wojcik, E. Gorecka, *ChemPhysChem* **2014**, *15*, 1283-95.
- [16] a) M. Wojcik, W. Lewandowski, J. Matraszek, J. Mieczkowski, J. Borysiuk, D. Pocięcha, E. Gorecka, *Angew. Chem. Int. Ed.* **2009**, *48*, 5167-5169; b) M. Wojcik, M. Kolpaczynska, D. Pocięcha, J. Mieczkowski, E. Gorecka, *Soft Matter* **2010**, *6*, 5397-5400.
- [17] a) X. Zeng, F. Liu, A. G. Fowler, G. Ungar, L. Cseh, G. H. Mehl, J. E. Macdonald, *Adv. Mater.* **2009**, *21*, 1746-1750; b) J. M. Wolska, D. Pocięcha, J. Mieczkowski, E. Gorecka, *Soft Matter* **2013**, *9*, 3005-3008; c) W. Lewandowski, K. Jatzczak, D. Pocięcha, J. Mieczkowski, *Langmuir* **2013**, *29*, 3404-3410.
- [18] a) W. Lewandowski, M. Fruhnert, J. Mieczkowski, C. Rockstuhl, E. Gorecka, *Nat. Commun.* **2015**, *6*, 6590; b) W. Lewandowski, T. Łojewska, P. Szustakiewicz, J. Mieczkowski, D. Pocięcha, *Nanoscale* **2016**, *8*, 2656-2663.
- [19] M. Brust, M. Walker, D. Bethell, D. J. Schiffrin, R. Whyman, *J. Chem. Soc. Chem. Commun.* **1994**, *7*, 801-802.
- [20] M. M. Wojcik, M. Olesinska, M. Sawczyk, J. Mieczkowski, E. Gorecka, *Chem - A Eur. J.* **2015**, *21*, 10082-8
- [21] A. Zep, M. M. Wojcik, W. Lewandowski, K. Sitkowska, A. Prominski, J. Mieczkowski, D. Pocięcha, E. Gorecka, *Angew. Chem. Int. Ed. Engl.* **2014**, *53*, 13725-8.
- [22] H. Sun, *J. Comput. Chem.* **1994**, *15*, 752-768.
- [23] M. J. Guberman-Pfeffer, J. Ulcickas, J. A. Gascón, *J. Phys. Chem. C* **2015**, *119*, 27804-27812.
- [24] a) J. Choi, H. Chung, J.-H. Yun, M. Cho, *Appl. Phys. Lett.* **2014**, *105*, 221906; b) J. Choi, H. Chung, J.-H. Yun, M. Cho, *ACS Appl. Mater. Interfaces* **2016**, *8*, 24008-24024.
- [25] J. Choi, H. Shin, S. Yang, M. Cho, *Compos. Struct.* **2015**, *119*, 365-376.
- [26] a) H. Finkelmann, G. Rehage, *Makromol. Chem., Rapid Commun.* **1980**, *1*, 31; b) P. Beyer, R. Zentel, *Macromol. Rapid Commun.* **2005**, *26*, 874-879; c) J. Kupfer, H. Finkelmann, *Makromol. Chem. Rapid Commun.* **1991**, *12*, 717; d) H. Kim, B. Zhu, H. Chen, O. Adetiba, A. Agrawal, P. Ajayan, J. G. Jacot, R. Verduzco, *J. Vis. Exp.* **2016**, *108*, e53688.
- [27] Ch. Ohm, M. Brehmer, R. Zentel, *Adv. Mater.* **2010**, *22*, 3366-3387.

FULL PAPER

Entry for the Table of Contents (Please choose one layout)

FULL PAPER



Homogeneous dispersion of metallic nanoparticles in polymer matrix has been achieved by using nanoparticles as exclusive cross-linkers in the preparation of LC elastomer. Chemical bonding of NPs prevented their agglomeration even after multiple temperature cycling through the smectic/liquid phase transition.

Michał M. Wójcik*, Jarosław Wróbel,
Zuzanna Z. Jańczuk, Józef
Mieczkowski, Ewa Górecka, Joonmyung
Choi, Maenghyo Cho, Damian
Pociecha*

Page No. – Page No.

Liquid crystalline elastomers with
gold nanoparticle cross-linkers